

# Electronic structure and optical properties of silicon nanowires: A study using x-ray excited optical luminescence and x-ray emission spectroscopy

T. K. Sham, S. J. Naftel, P.-S. G. Kim, R. Sammynaiken, and Y. H. Tang  
*Department of Chemistry, University of Western Ontario, London, Canada N6A 3B7*

I. Coulthard  
*The Canadian Light Source, University of Saskatchewan, Saskatoon, Canada*

A. Moewes  
*Department of Physics, University of Saskatchewan, Saskatoon, Canada*

J. W. Freeland  
*Advanced Photon Source, Argonne National Laboratory, Argonne, Illinois 60439, USA*

Y.-F. Hu  
*Canadian Synchrotron Radiation Facility, Synchrotron Radiation Center, University of Wisconsin, Madison, Wisconsin 53589, USA*

S. T. Lee  
*Center of Super-Diamond and Advanced Films (COSDAF) and Department of Physics and Materials, City University of Hong Kong, Hong Kong SAR, China*

(Received 19 November 2003; revised manuscript received 12 March 2004; published 20 July 2004)

We report a soft x-ray excited optical luminescence (XEOL) and x-ray emission spectroscopy (XES) study of silicon nanowires (SiNW) with excitations at the silicon  $K$  and  $L_{3,2}$  edge, respectively. It is found that the XEOL of SiNW exhibits several luminescence bands at  $\sim 460$ ,  $\sim 530$ , and  $\sim 630$  nm. These luminescence bands are broad and are sensitive to the Si  $1s$  excitation channel (Si versus  $\text{SiO}_2$  whiteline). These chemical- and morphology-dependent luminescences are attributable to the emission from the encapsulating silicon oxide, the quantum-confined silicon crystallites of various sizes embedded in the oxide layer, and the silicon-silicon oxide interface. XES clearly shows the presence of a relatively thick oxide layer encapsulating the silicon nanowire and the densities of states tailing across the Fermi level. The implications of these findings to the electronic and optical properties of silicon nanowires are discussed.

DOI: 10.1103/PhysRevB.70.045313

PACS number(s): 78.67.Lt, 78.55.Ap, 78.70.Dm, 78.70.En

## INTRODUCTION

The discovery of luminescence from porous silicon,<sup>1</sup> a mesoporous network of interconnecting silicon nanowires with pillars and nodules of the size of the order of nm (a quantum sponge), and the observation of light-emitting properties from a Si-based multiplayer superlattice (quantum-wells)<sup>2</sup> and nanoclusters (quantum dots)<sup>3,4</sup> have led to a large amount of exciting research.<sup>5</sup> The interest arises from the observation that bulk silicon, an indirect band gap material, does not exhibit luminescence in the visible spectrum, whereas porous silicon and other silicon nanostructures do, even at room temperature.<sup>1-5</sup> Thus, there is a great potential to develop nanoelectronic devices with silicon nanostructures. More recently, techniques to fabricate silicon nanowire, a very desirable configuration for nanodevice interconnect applications, were reported.<sup>6,7</sup> In addition to photoluminescence, all of the above-described Si nanostructures have the following two features in common: (a) they all contain quantum-confined elemental silicon structures of the order of nm dimension, and (b) they are often capped by silicon oxide. The light-emitting properties of porous silicon, silicon superlattices, and nanoclusters, are reasonably well studied.<sup>3-5,8</sup> The luminescence exhibits a wide range of crys-

tallite size-dependent blue shifts relative to the indirect band gap energy of bulk silicon (1.1 eV), due to quantum confinement that opens the band gap when the size becomes significantly small (of the order of nm).<sup>5</sup> In addition, the capping oxide layer is amorphous and contains suboxides and oxide, which also contribute to the luminescence.<sup>8-11</sup> It is expected that the light-emitting properties of silicon nanowires are similar to that of other Si nanostructures, although relatively few studies are known.<sup>11,12</sup> In this paper, we report a study of silicon nanowire (henceforth denoted SiNW) using two photon-in photon-out techniques: x-ray excited optical luminescence (XEOL)<sup>8,13</sup> and x-ray emission spectroscopy (XES).<sup>3,14-17</sup>

The XEOL technique monitors the optical response of a light-emitting material by tuning the x ray to the energy of a specific excitation channel (e.g., the  $K$ -edge threshold at  $\sim 1839.6$  eV corresponds to the excitation of a  $1s$  electron in crystalline Si to the bottom of the conduction band) and monitoring the luminescence with an optical monochromator, typically in a range of 200–900 nm. When the excitation photon energy is tuned across an absorption edge, the atom of interest absorbs an increasing fraction of the incoming photons abruptly (an edge jump), exciting a core electron

to an previously unoccupied state above the Fermi level. Thus, the involvement of an atomic orbital of the absorbing atom in the excited state [e.g., the partial densities of states of a Si  $3p$  character in the conduction band, or the contribution of a carbon  $2p$  orbital to the LUMO (lowest unoccupied molecular orbital)] in the luminescence chromophore [the band gap or the LUMO-HOMO (highest occupied molecular orbital) emission] will contribute to the site and excitation channel specificity of the luminescence.<sup>18,19</sup> The relative quantum yield of the luminescence chromophore, which is either due to the recombination of a hole ( $h$ ) in the valence band and an electron ( $e$ ) in the conduction band, or due to defects, can be monitored through these site and excitation channel specific processes.

In the soft x-ray region, this technique is very desirable because the excitation is often associated with shallow cores. These levels are generally immediately below the valence band, and have large cross sections and a narrow lifetime broadening for high-sensitivity spectroscopic studies. The threshold excitation of shallow cores creates a core hole and an electron in the previously unoccupied state above the Fermi level (or LUMO and LUMO plus in molecules). The core hole is unstable and is filled in a deexcitation process with electrons from the inner valence and the valence shells leaving holes behind. This primary process results in holes in the valence band (HOMO in molecules) and electrons in the conduction band (LUMO in molecules), which can recombine radiatively. The Auger electrons associated with the corehole decay can also create holes and electrons in the valence band and the conduction band, respectively, as they thermalize in the solid. In soft x-ray excitation, Auger decay is the dominant deexcitation process and the Auger electrons are of relatively low energy and the secondary process has a short attenuation length, typically of the order of 1 nm. Thus, both the primary and secondary processes provide a high degree of site specificity. Similar arguments apply to the formation and deexcitation of excimers, exciplexes, and defects of which the quantum yield depends on the nature of the excited state.<sup>18,19</sup>

The photoluminescence yield (PLY) can in turn be used to record x-ray absorption fine structure (XAFS) that provides structural information for the absorption site that is responsible for the luminescence.<sup>8</sup> As noted above, XEOL is particularly sensitive in the soft x-ray region where secondary processes, which also contribute to luminescence, have short attenuation lengths.

In XES, the fluorescence x rays from the decay of a shallow core hole produced by the absorption of x rays, is measured.<sup>15,16</sup> If the core level is just below the valence band, the XES maps the densities of states (DOS) of the valence band (e.g., the XES from the decay of the Si  $L_{3,2}$ -core hole of Si yields the partial DOS of the valence band of Si).<sup>3,15-17</sup> It is a desirable alternative to photoemission measurements, since nanostructures often exhibit serious charging behavior due to a Coulomb blockade, and the relatively large escape depth of the emitted photons allows us to see through the encapsulating layers.

## EXPERIMENT

The SiNW specimens used in this investigation were prepared with a laser ablation technique, as described in a recent

study of the electronic structure of a similar batch of samples.<sup>7</sup> The specimen investigated here has a nominal diameter of  $\sim 13$  nm, of which there is a silicon oxide outer layer of  $\sim 3-4$  nm, as revealed by TEM.<sup>12,20</sup> It is well documented that the morphology of SiNW depends on the method of preparation.<sup>6,12</sup> It should also be noted that SiNW specimens, even from the same preparation, comprise a distribution of wires of slightly different size and morphology. Thus the XEOL results, unlike high-resolution TEM, which looks at a single wire, represent the average optical properties of the SiNW specimen under investigation. The XEOL of the as-prepared SiNW, dispersed on a stainless steel substrate and excited with selected photon energies across the Si  $K$  edge, were first obtained at the 4-ID-C spherical grating monochromator (SGM) beamline of the Advanced Photon Source (APS) at the Argonne National Laboratory using a very small beam ( $\sim 0.1$  mm), and later at the Double Crystal Monochromator (DCM) beamline of the Canadian Synchrotron Radiation Facility (CSR) at the Synchrotron Radiation Center (SRC), University of Wisconsin-Madison, using a much bigger beam (several mm). Both measurements yield similar results at first glance. A close examination reveals some noticeably different features, which reflect the chemically inhomogeneous morphology and the nanocomposite nature of the specimen (see below). The XEOL of the same specimen, before and immediately after a HF treatment for the removal of the surface oxide, was obtained at SRC.

Figure 1 shows the high-resolution transmission electron microscopy (HRTEM) and energy dispersive x ray (EDX) of a typical SiNW before and after HF treatment. The HF procedure in this case clearly shows that the technique removes most of the surface oxide and that the crystalline nature of the SiNW remains intact. It must be noted that, due to the size distribution and the variable morphology, it is difficult to remove all the oxides from all the nanowires in a macroscopic specimen such as the one used in the present measurement without washing away a considerable amount of samples. Thus, a mild treatment was used here to ensure that some oxides are removed, but there is still enough sample remaining to provide sufficient sensitivity. The XES of a specimen from the same batch was obtained at the BL 8.0.1 of the Advanced Light Source (ALS) at Lawrence Berkeley National Laboratory.

## RESULTS AND DISCUSSION

Figure 2 shows the XEOL of SiNW excited with photon energies from below to above the Si  $K$  edge. The Si  $K$ -edge x-ray absorption near edge structure (XANES) is shown in inset (a). The first resonance above the edge probes the Si  $3p$  character in the conduction band of the elemental Si in SiNW. In bulk silicon, this peak appears as a doublet (band structure effect) that blurs in nano silicon.<sup>5,20</sup> The intense peak at 1847.5 eV is the SiO<sub>2</sub> whiteline (WL) arising from a  $1s$  to  $t_2$  ( $p$  character) transition of Si in a local  $T_d$  oxygen environment.

It should be noted that the site and channel specific excitations discussed here are the dominant excitation channels, but they are not the only channels that are excited at that

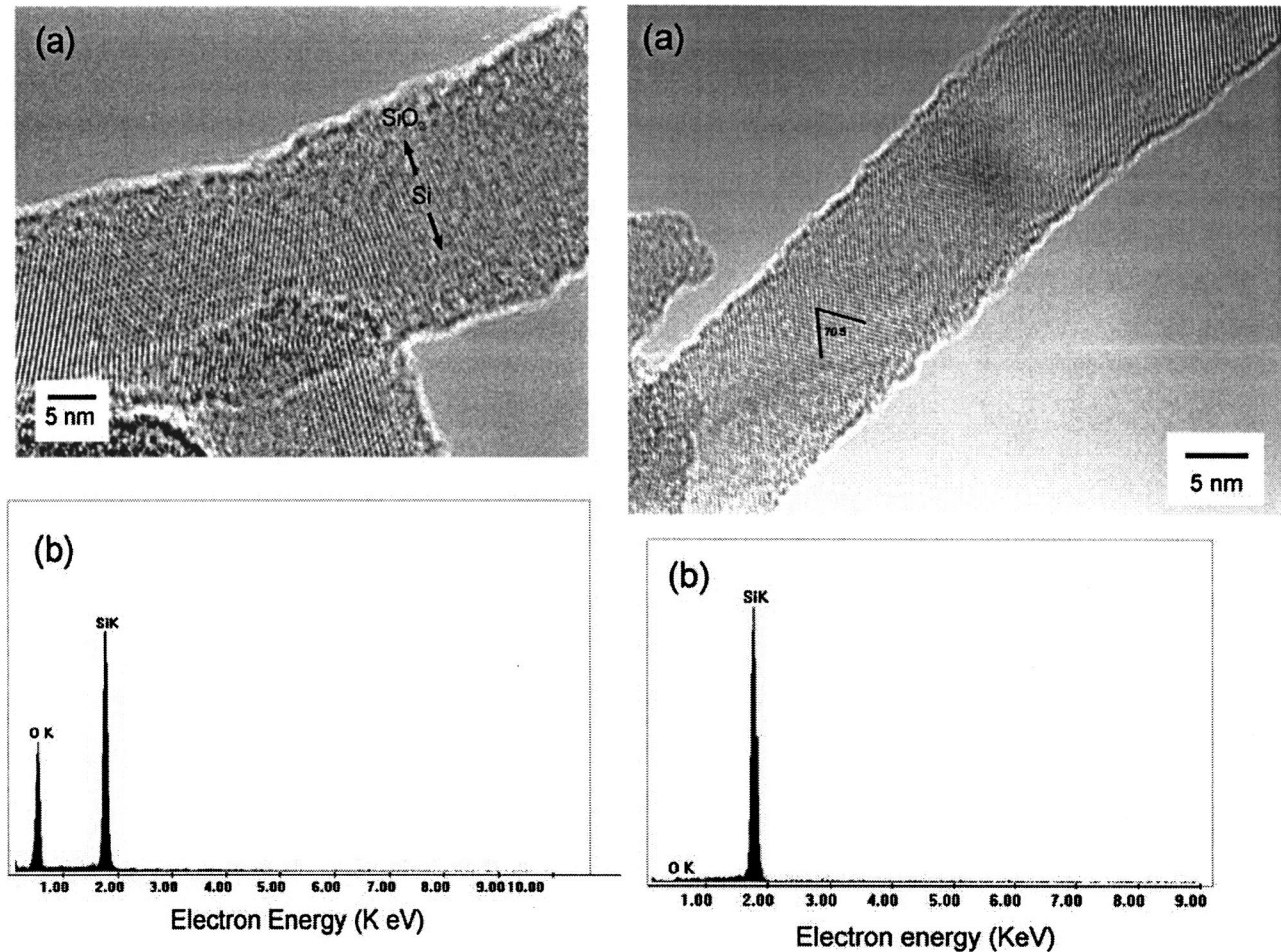


FIG. 1. The TEM and EDX of SiNW, shown in the left panel as prepared and in the right panel after HF treatment.

energy. For example, below the Si  $K$  edge (e.g., 1830 eV), all the Si  $2p$ ,  $O1s$ , and valence band electrons are excited to the continuum, and the radiative deexcitation produces luminescence. At the first WL (1842 eV), the Si  $1s$ - $p$  DOS transition of elemental Si turns on, and absorbs most of the incoming photons, since its cross section is much larger than that of the shallower levels and the valence band. At 1847.5 eV, the  $1s$ - $3p$  transition of the silicon oxide becomes a dominant channel, the  $1s$  upper-band transition for the elemental Si, though less competitive, still takes place.

The luminescence spectra (normalized to photon flux,  $I_0$ ) in Fig. 2 show three major broad bands at  $\sim 460$  nm (2.7 eV), 530 nm (2.34 eV) and 630 nm (1.97 eV). The intensity and the branching ratio of the 2.7 eV peak reaches a maximum when the  $K$  edge channel of silicon oxide turns on at 1847.5 eV. This is illustrated in inset (b) by the difference curve (peaks at 460 nm) between the 1847.5 eV ( $\text{SiO}_2$  WL) and the 1842 eV (Si WL)-excited luminescence. We attribute the 2.7 eV peak to the luminescence from defects of the encapsulating oxide. This 2.7 eV luminescence is commonly observed in silica glass, and has been attributed to the triplet-to-ground-state luminescence from a  $\text{SiO}_2$  defect involving a bridging oxygen vacancy between two adjacent Si ( $\equiv\text{Si}-\text{Si}\equiv$ ).<sup>21-24</sup> Luminescence at similar wavelengths has also been observed in porous silicon

and solution-grown SiNW.<sup>11,12,22-25</sup> It should be noted that above the Si threshold and below the  $\text{SiO}_2$  WL, [inset (a)], elemental Si absorbs most of the photons. However, when the silicon oxide channel turns on, both the Si and  $\text{SiO}_2$  are competing for the incoming photons. The absorption at the  $\text{SiO}_2$  WL will facilitate luminescence from the oxide chromophore if the process has a high quantum yield, as is observed.

It is also of interest to ask whether or not the  $\sim 460$  nm band can have its origin in elemental silicon as well, since Si nanostructure is known to have a widely tunable range in its photoluminescence,<sup>5</sup> and the intensity of the 460 nm band is noticeable when excited at the elemental Si channel (1842 eV). A comparison of the luminescence from 1830 eV (below the Si  $K$  edge) to 1842 eV (elemental Si WL) excitation clearly shows an enhancement in the branching ratio of the 460 nm peak, suggesting that small Si nanocrystallites also contribute to the luminescence in this region. In fact, it has been observed that porous silicon exhibits overlapping silicon oxide and nanosilicon luminescence bands.<sup>21</sup> It is interesting to note that the site specificity of XEOL in SiNW is less dramatic than in porous silicon.<sup>8</sup> This may be attributable to the low quantum yield of the crystalline Si in the core of the SiNW, of which the size is too large to exhibit the quantum confinement effect.

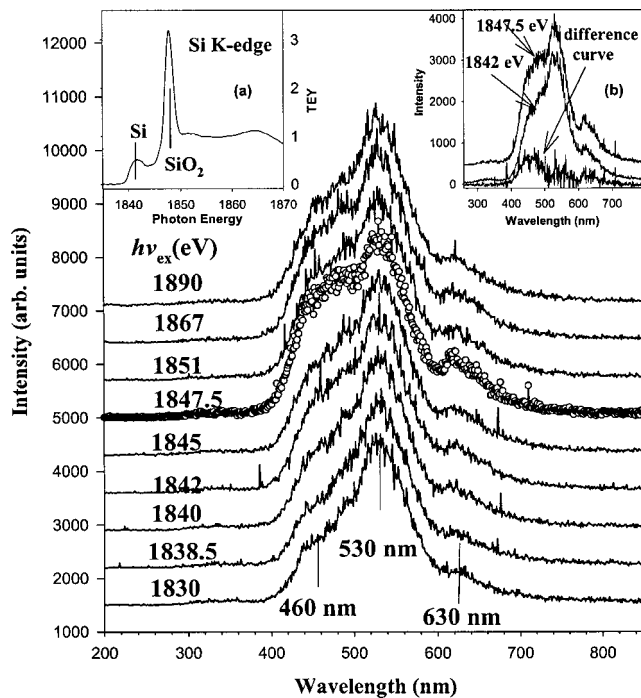


FIG. 2. Normalized XEOL of SiNW excited at photon energy across the Si *K* edge. The TEY XANES and the difference curve between the luminescence of the SiO<sub>2</sub> and Si white line excitation channel are shown in insets (a) and (b), respectively. The baselines have been shifted vertically for clarity. The dark count is  $\sim 150$  counts/s.

Figure 3 shows the PLY of the Si *K*-edge XANES monitored with total (zero order) and wavelength-selected luminescence. The total electron yield (TEY) and fluorescence yield (FLY) XANES are also shown. We see that in the surface-sensitive TEY (probing depth  $\sim$  nm), the edge-jump ratio of silicon/oxide is  $\sim 1:1$  and increases to  $\sim 2.5:1$  in FLY and zero-order PLY (probing depth  $\sim 10$ – $10^2$  nm).<sup>9</sup> The edge jumps of the latter two are good representations of the composition, since these techniques are more bulk sensitive. The most interesting features are seen in the wavelength-selected PLY, where the 460 nm (2.7 eV) PLY exhibits the most intense oxide WL (SiO<sub>2</sub>/Si WL height ratio = 1.3, compared to 1:1 in FLY and 0.9:1 in zero-order PLY), whereas the 530 nm PLY is the least intense (SiO<sub>2</sub>/Si WL height ratio = 0.6). This observation indicates that the luminescence at 460 nm (2.7 eV) favors a silicon oxide origin, while the 530 nm (2.33 eV) peak is attributable to elemental Si. It should be cautioned, however, that the intensity of the elemental resonance (1842 eV) in the 460 nm yield is still quite strong, indicating that luminescence at this wavelength from still smaller crystallites is probable. We will return to this point later.

The photoluminescence observed here is significantly blue shifted, relative to the indirect band gap of bulk silicon (1.1 eV) and that of typical porous silicon samples (600–700 nm or 2.07–1.77 eV), but is within range of the direct gap at the  $\Gamma$  point of the Si band structure and what has been observed in many nanosilicon systems with a small crystallite size.<sup>5,22</sup> We attribute the 530 nm peak to the

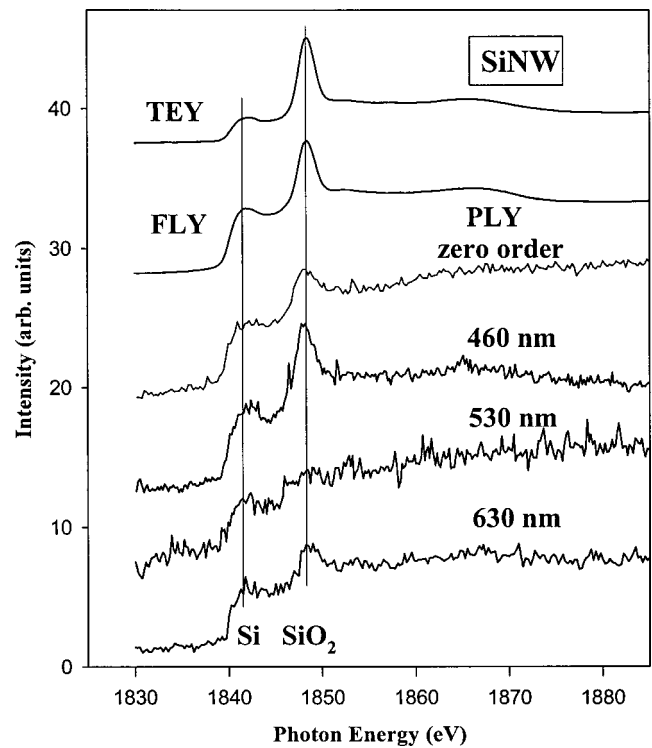


FIG. 3. Si *K* edge XANES of Si nanowire obtained with TEY, FLY, zero-order PLY, and wavelength-selected PLY (at APS).

electron-hole recombination in small crystallites that are embedded in the oxide layer of the SiNW, instead of the Si core. This is because the required crystallite size to exhibit luminescence, based on the quantum-confinement model, has to be significantly smaller than the diameter of the nanowire ( $\sim 10$  nm). For example, a 2.33 eV (530 nm) gap would correspond to a  $\sim 2$  nm crystallite according to recent experiment and theory.<sup>26–30</sup> The 630 nm luminescence is less sensitive to the excitation energy (SiO<sub>2</sub>/Si WL height ratio  $\sim 0.8$ ) and is attributed to interface defects between Si and silicon oxide, and suboxide and quantum-confined silicon crystallites with a slightly larger size ( $> 2$  nm). This notion is also borne out in the increasing luminescence intensity going from excitation at the Si *K* edge (1842 eV) to above the edge, as shown in Fig. 2 (inset).

Figure 4 shows the XEOL of the SiNW recorded at SRC, before and after the specimen was treated with a HF solution. The corresponding TEY is shown in the inset. The HF procedure was intended to remove the surface oxide, which is relatively thick (several nm, see Fig. 1), and is often an essential part of the growth of SiNW.<sup>12</sup> Before HF treatment, the spectra for the as-prepared samples are, at first glance, similar to those recorded at the APS. A close examination reveals a noticeable but significant difference, which is attributed to the combined effect of the sampling of a much larger area (several tens) of the specimen in the SRC experiment, the ambient atmosphere, and the slightly different experimental configuration. The differences and their implications are addressed below.

Figure 5 compares the XEOL of the APS (Fig. 2) and the SRC (Fig. 4) experiments excited at the silicon oxide, and

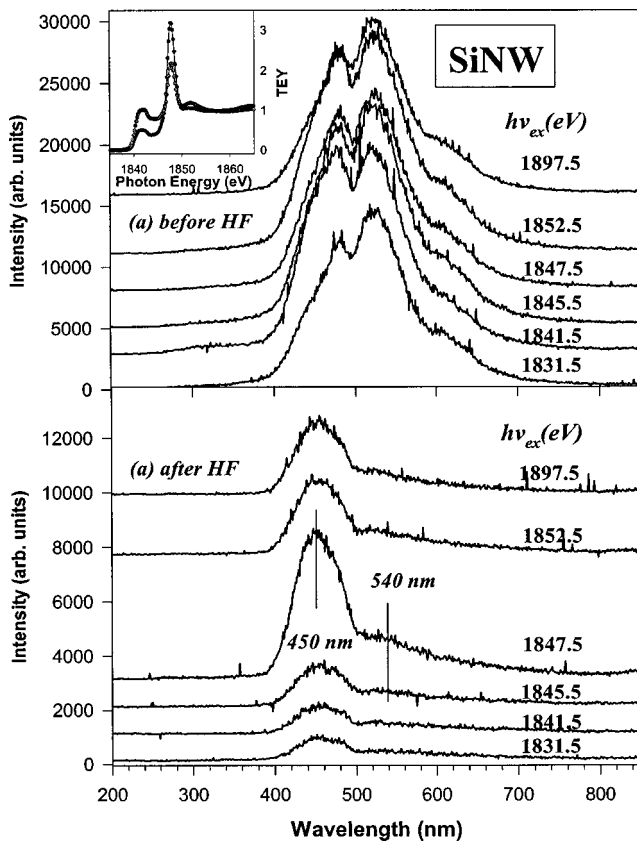


FIG. 4. Normalized XEOL of SiNW before (top) and after (bottom) HF treatment (at SRC). The TEY XANES before (solid circle) and after the HF treatment (open circle) is shown in the inset. The baselines have been shifted vertically for clarity.

the elemental silicon WL excitation channel just above the Si  $K$  edge. As noted above, the difference between these two experiments is that the latter samples a much larger area and that the specimen had been stored in the ambient for a period of time (several months) after the APS run. It can be seen that at the 1847.5 eV excitation (the dominant SiO<sub>2</sub> channel), both experiments show very similar results. However, the 1841.5 eV excitation (elemental Si nanostructure channel) reveals a significant difference, i.e., that the short wavelength band from the SRC run is sharper, and the maximum is identified at  $\sim$ 480 nm. Also, its branching ratio is considerably larger than that of the APS run. In fact, it shows the opposite trend of that of the APS result (Fig. 2, inset b). This observation indicates that the morphology of the SiNW, on average, and hence the luminescence properties we were measuring in the SRC run, are not exactly the same as the region of the specimen we sampled in the APS run. This is possible, given the distribution of sizes and morphology in a macroscopic sample, the much larger sampling area in the SRC experiment, and that the sample had been irradiated and then stored in the ambient for months, which may result in further oxidation.

Figure 6 shows a comparison of the XEOL excited with 1847.5 and 1841.5 eV photons from the SRC experiment before and after the HF treatment, and corresponding difference curves (oxide-Si excitation). Before HF treatment, the

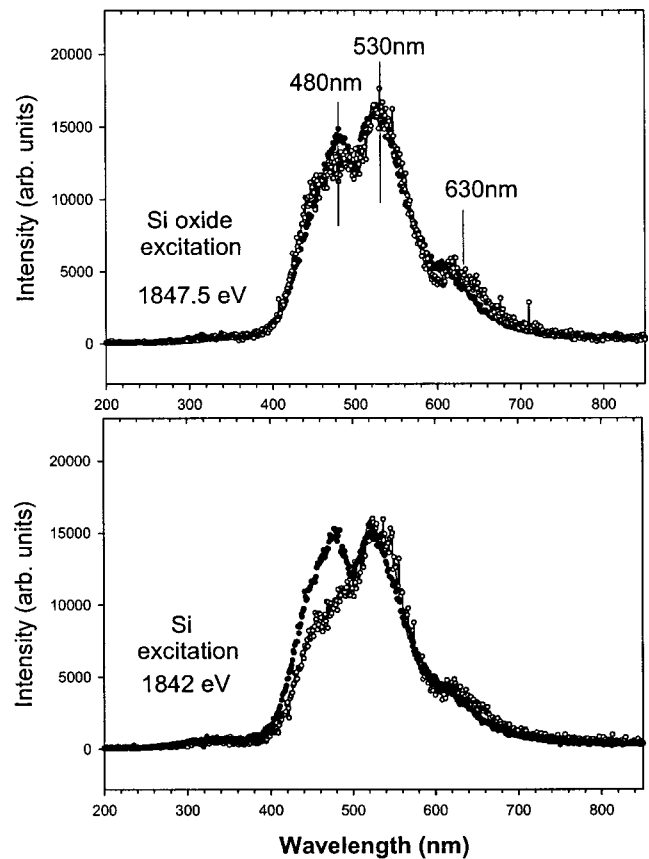


FIG. 5. A comparison of XEOL recorded at APS and SRC excited at 1847.5 and 1842 eV. The open circles represent the APS data; the black circles represent the SRC data.

difference curve reveals an emission at 440 nm, which has a maximum branching ratio at 1841.5 eV (the elemental Si) excitation. This peak can be associated with the emission from still smaller Si nanostructures ( $<2$  nm) embedded in the amorphous silicon layer, which was then washed away upon HF treatment. After HF, the difference curve clearly shows the dramatic enhancement of luminescence at 450 nm when the excitation energy changes from 1841.5 to 1847.5 eV (the silicon oxide channel). Thus, for the HF treated sample, the 450 nm can be attributed to oxide luminescence with confidence. The 530 nm peak was also enhanced, but with a smaller branching ratio, consistent with an earlier assignment to small Si nanoparticles.

Returning to Fig. 4, several other spectral changes after HF can be identified. First, the edge jump for the elemental Si (inset) increases by a factor of  $\sim$ 4 relative to the oxide, although as can be inferred from the SiO<sub>2</sub> whiteline at 1847.5 eV, a considerable amount of oxide remains. It should be reiterated that as attempt to remove all surface oxides with an excessive hf treatment would likely wash away the specimen entirely, since the macroscopic specimen contains a distribution of SiNW of a slightly different size and morphology. Thus, a modest HF treatment was applied, which did not completely remove all the surface oxide. Second, the overall luminescence intensity decreases by an order of magnitude after the HF treatment, consistent with the fact that some samples were dissolved and washed away. Third,

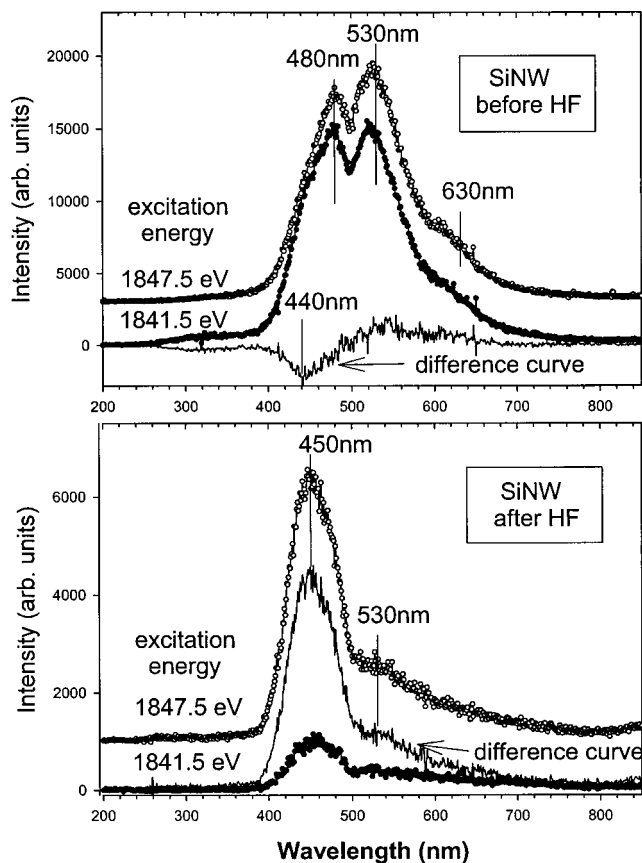


FIG. 6. A comparison of the XEOL data from SRC excited at 1847.5 eV (oxide) and 1841.5 eV (elemental) excitation channels. The difference curves are also shown.

in addition to the luminescence at  $\sim 450$  nm, of which the branching ratio increases dramatically at the silicon oxide whiteline (1847.5 eV) as noted above (Fig. 6), the 530 nm emission becomes less intense and the 630 nm peak becomes a tailing feature. We attribute this observation to the loss of both Si nanocrystallites and silicon oxide luminescence sites due to HF treatment, which might also introduce new defects. However, the HF must have removed a significant portion of the nano Si crystallites, and the associated silicon-oxide interface (suboxide) in the amorphous silicon oxide layer responsible for the 440 and 530 nm, and the 630 nm luminescence, respectively. This suggests that the smaller Si nanoparticles are very close to the surface of the oxide layer. The silicon oxide excitation channel enhanced luminescence at 450 nm after the HF observed in Figs. 4 and 6 must come from the remaining oxide layer on the SiNW surface (inset, Fig. 4). The corresponding PLY XANES shown in Fig. 7 also reflect the dominance of the oxide luminescence, as the photoluminescence response to the silicon oxide whiteline excitation is clearly present in all luminescence channels, including the 530 nm, which is now a minor component, and overlaps with the tail of the intense oxide luminescence. The elemental Si WL observed in the PLY must arise largely from the secondary contribution of the absorption of the core silicon, of which the dimension is too large to exhibit the effect of quantum confinement.

The oxide origin of the 460 nm luminescence was recently demonstrated in a chainlike silicon nanowire prepared

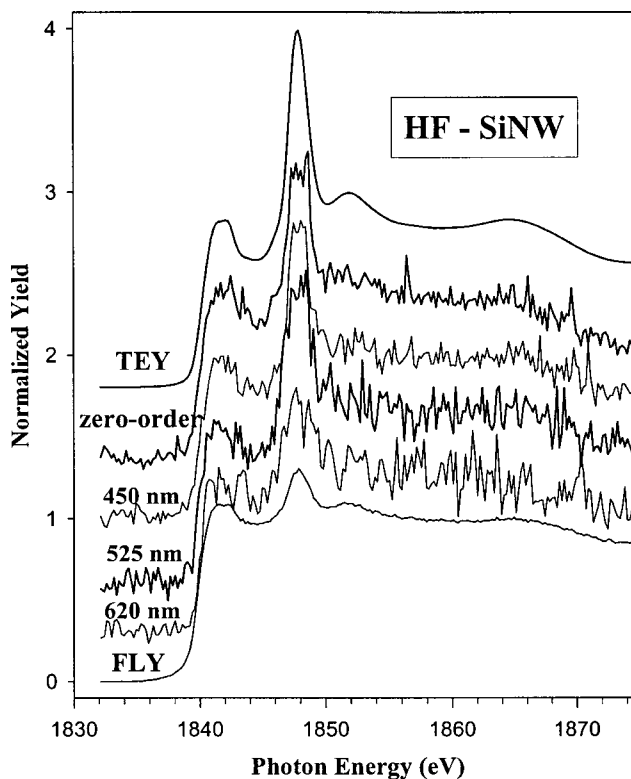


FIG. 7. Si *K*-edge XANES of HF-treated SiNW with TEY, FLY, and PLY (total and wavelength selected).

by a thermal evaporation method with a fluctuating carrier gas pressure.<sup>30</sup> This type of SiNW consists of an amorphous silicon oxide chain linking Si nanoparticles of the size of several nm. These particles are totally embedded in the amorphous silicon oxide chain with a nominal diameter of  $\sim 16$  nm and a separation of  $\sim 20$  nm between Si nanoparticles. Figure 8 shows the XEOL of the chainlike SiNW excited at the SiO<sub>2</sub> (1848 eV) and the elemental Si (1841 eV) resonance. It looks remarkably similar to the HF-treated SiNW (Figs. 4 and 6), while the elemental Si edge jump in the 460 nm PLY (not shown) of this oxide-dominated specimen is negligible,<sup>30</sup> unlike Fig. 6.

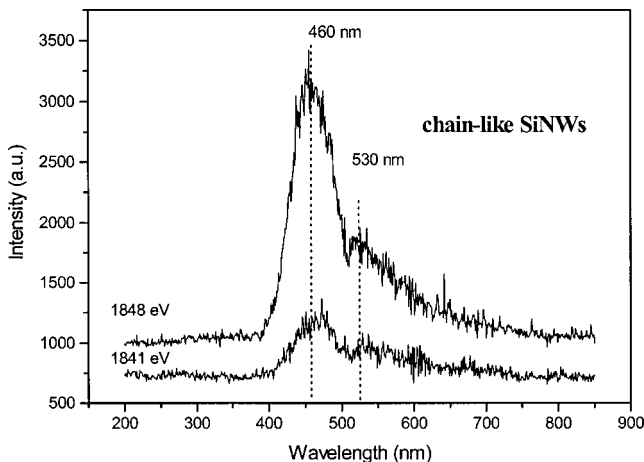


FIG. 8. Si *K*-edge excited XEOL of a chain like SiNW excited at the oxide and the elemental channel.

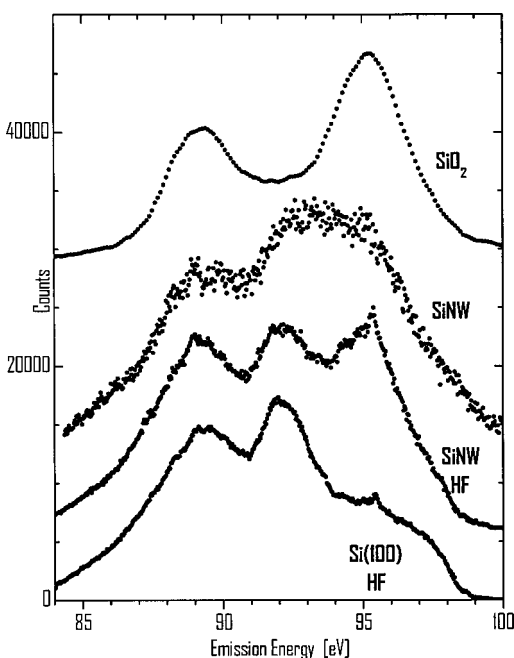


FIG. 9. The calibrated XES of SiNW, HF-treated SiNW, and clean Si(100). The baselines have been shifted vertically for clarity. The SiO<sub>2</sub> XES is also shown.

We also investigated the valence electron density distribution of the SiNW. XES was preferred over photoemission due to the charging problem of SiNW.<sup>20</sup> Figure 9 shows the Si  $L_{3,2}$  XES of the SiNW specimen before and after HF treatment together with that of a clean Si(100) and a SiO<sub>2</sub> specimen. The spectra were excited with a photon energy of 110 eV, which is above the Si  $L_{3,2}$  threshold of both elemental silicon and silicon oxide, and has an energy resolution of 150 meV. The broad band at the highest photon energy corresponds to the top of the valence band. More detailed results

of the XES at resonance will be dealt with elsewhere.<sup>31</sup> The Si(100) spectrum shows a three-peak pattern characteristic of the  $sp$  band of bulk silicon below the Fermi level.<sup>14–17</sup> The SiNW XES exhibits several interesting features. First, the as-prepared SiNW has a significant amount of oxide, as can be seen in the region closest to the Fermi level. Second, there are densities of states tailing towards the Fermi level, which exhibits a non-Fermi behavior, and diminishes upon HF treatment; we attribute these to interfacial states between elemental Si crystallites and silicon oxide. Finally, the crystalline Si XES features emerge after HF treatment. These observations confirm previous TEM results and the importance of the role of oxide layer in the growth of SiNW.<sup>12</sup>

## CONCLUSION

We have reported the XEOL of SiNW excited at selected photon energies across the Si  $K$  edge and shown that the luminescence from these SiNW specimens originated primarily from oxygen deficient sites in the encapsulating oxide, and from the quantum-confined silicon nanocrystallites encapsulated in the oxide layer. Both XEOL and XES show that the surface oxide plays a significant role in the electronic structure and optical properties of SiNW. This was recently confirmed in a related study.<sup>32</sup>

## ACKNOWLEDGMENTS

Research at the University of Western Ontario and the University of Saskatchewan is supported by NSERC of Canada. APS and ALS are supported by the US DOE under Contract No. W-31-109-Eng-38, and Contract No. AC03-76SF00098, respectively. CSRF is supported by NRC and NSERC of Canada. SRC is supported by the US NSF (DMR-0084402). Research at the City University of Hong Kong is supported by the GRC of Hong Kong.

- <sup>1</sup>L. T. Canham, *Appl. Phys. Lett.* **57**, 1046 (1990).
- <sup>2</sup>Z.-H. Lu, D. J. Lookwood, and J. M. Barbeau, *Nature (London)* **378**, 258 (1995).
- <sup>3</sup>T. van Buuren, L. N. Dinh, L. L. Chase, W. J. Siekhaus, and L. T. Terminello, *Phys. Rev. Lett.* **80**, 3803 (1998).
- <sup>4</sup>J. P. Wilcox and G. A. Samara, *Appl. Phys. Lett.* **74**, 3164 (1999).
- <sup>5</sup>A. G. Cullis, L. T. Canham, and P. D. J. Calcott, *J. Appl. Phys.* **82**, 1 (1997).
- <sup>6</sup>A. Morales and C. M. Lieber, *Science* **279**, 208 (1998).
- <sup>7</sup>Y. F. Zhang, Y. H. Tang, N. Wang, D. P. Yu, C. S. Lee, I. Bello, and S. T. Lee, *Appl. Phys. Lett.* **72**, 1835 (1998).
- <sup>8</sup>T. K. Sham, D. T. Jiang, I. Coulthard, J. W. Lorimer, X. H. Feng, K. H. Tan, S. P. Frigo, R. A. Rosenberg, D. C. Houghton, and B. Bryskiewicz, *Nature (London)* **363**, 331 (1993).
- <sup>9</sup>D.-T. Jiang, I. Coulthard, T. K. Sham, J. W. Lorimer, S. P. Frigo, R. A. Rosenberg, D. C. Houghton, and B. Bryskiewicz, *J. Appl. Phys.* **74**, 6335 (1993).
- <sup>10</sup>I. Coulthard, D. T. Jiang, and T. K. Sham, *J. Electron Spectrosc.*

- Relat. Phenom.* **79**, 233 (1996).
- <sup>11</sup>J. D. Holmes, K. P. Johnston, R. C. Doty, and B. A. Korgel, *Science* **287**, 1471 (2000).
- <sup>12</sup>S. T. Lee, N. Wang, Y. F. Zhang, and Y. H. Tang, *MRS Bull.* **24**, 36 (1999).
- <sup>13</sup>A. Rogalev and J. Goulon in *Chemical Application of Synchrotron Radiation*, edited by T. K. Sham (World Scientific, Singapore, 2002), Part II, p. 707.
- <sup>14</sup>J. E. Rubensson, D. Mueller, R. Shuker, and D. L. Ederer, *Phys. Rev. Lett.* **64**, 1047 (1990).
- <sup>15</sup>A. Moewes, E. Z. Kumaev, J. S. Tse, M. Geshi, M. J. Ferguson, V. A. Trofimova, and Y. M. Yarmoshenko, *Phys. Rev. B* **65**, 153106 (2002).
- <sup>16</sup>E. J. Nordgren, S. M. Butorin, L. C. Duda, J.-H. Guo, and J.-E. Rubensson in *Chemical Applications of Synchrotron Radiation*, edited by T. K. Sham (World Scientific, Singapore, 2002), Part I, p. 517.
- <sup>17</sup>S. Eisebitt, J. Luning, J.-E. Rubensson, W. Eberhardt, M. Berger, R. Arens-Fischer, T. van Buuren, S. N. Patitsas, and T.

- Tiedje, *Solid State Commun.* **97**, 549 (1996).
- <sup>18</sup>S. J. Naftel, P. S. G. Kim, T. K. Sham, R. Sammynaiken, B. W. Yates, and Y.-F. Hu, *J. Appl. Phys.* **93**, 5191 (2003).
- <sup>19</sup>P.-S. G. Kim, M.-C. Brandys, Y.-F. Hu, R. J. Puddephatt, and T. K. Sham, *J. Lumin.* **105**, 21 (2003).
- <sup>20</sup>Y. F. Zhang, L. S. Liao, W. H. Chan, R. Sammtnaikin, S. T. Lee, and T. K. Sham, *Phys. Rev. B* **61**, 8298 (2000).
- <sup>21</sup>I. Coulthard, W. J. Antel, Jr., J. W. Freeland, T. K. Sham, S. J. Naftel, and P. Zhang, *Appl. Phys. Lett.* **77**, 498 (2000).
- <sup>22</sup>M. V. Wolkin, J. Jorne, P. M. Fauchet, G. Allan, and O. Delerue, *Phys. Rev. Lett.* **82**, 197 (1999).
- <sup>23</sup>R. Tohmon, Y. Shimagaichi, H. Mizuno, and Y. Ohki, *Phys. Rev. Lett.* **62**, 1388 (1989).
- <sup>24</sup>J. H. Stathis and M. A. Kastner, *Phys. Rev. B* **35**, 2972 (1987).
- <sup>25</sup>Oxidized Si nanostructures often exhibit multiple luminescence peaks both in the UV and in the visible spectrum, of which the light-emitting mechanism is complex and the oxide luminescence can be as important, or even more important, than the luminescence from the oxygen-capped Si nanostructure. What is unique in SiNW is that the oxide was already acquired during the fabrication, while in porous silicon the oxides are often the results of surface oxidation.
- <sup>26</sup>X.-H. Sun, Y. H. Tang, P. Zhang, S. J. Naftel, R. Sammynaikin, T. K. Sham, H. Y. Peng, Y.-F. Zhang, N. B. Wong, and S. T. Lee, *J. Appl. Phys.* **90**, 6379 (2001).
- <sup>27</sup>S. Ögüt, J. R. Chelikowsky, and S. G. Louie, *Phys. Rev. Lett.* **79**, 1770 (1997).
- <sup>28</sup>G. Allan, C. Delerue, and M. Lannoo, *Phys. Rev. Lett.* **76**, 2961 (1996).
- <sup>29</sup>P. E. Batson and J. R. Heath, *Phys. Rev. Lett.* **71**, 911 (1993).
- <sup>30</sup>X. H. Sun *et al.*, *J. Appl. Phys.* (to be published).
- <sup>31</sup>A. Moewes *et al.* (unpublished).
- <sup>32</sup>R. A. Rosenberg, G. K. Shenoy, and T. K. Sham (unpublished).